The Optimal Echo Time Setting on Heavily T2-Weighted Fluid Attenuated Inversion Recovery Images for Detecting Very Low Concentrations of Gadolinium-Based Contrast Agent in the Brain: A Phantom Study

Yusuke Sato[1,2] · Norio Hayashi[3] · Kouichi Ujita[1] · Takayuki Suto[1] · Haruyuki Watanabe[3] · Yoshito Tsushima[4]

Abstract

A heavily T2-weighted FLAIR (hT2W-FLAIR) may have a potential to visualize very low concentration of gadolinium (Gd)-based contrast agents (GBCAs), owing to the water-suppression pulse and the decreased parenchymal signal due to a long echo time (TE). However, the optimal TE setting has not been well established. Our study aimed to elucidate the optimal TE for visualizing very low concentrations of GBCA in a phantom study. We employed phantoms made of diluted gadobutrol (Gd-BTDO3A) and purified water (4–128 μM), simulating cerebrospinal fluid (CSF), gray matter and white matter. The hT2W-FLAIR images were acquired using a 1.5-T MRI scanner, and the TE was changed in 100 ms increments from 100 to 800 ms. The acquired images were evaluated with the contrast-to-noise ratio (CNR) for the CSF phantom. The CNRs of the gray and white matter decreased steeply when the TE exceeded. However, the CNRs of GBCA did not depend on the TE setting for all concentrations, and were significantly higher than those of the gray or white matter at the TE of 500–800 ms for 32–128 μM ($p < 0.05$). At a TE of 700 ms, the CNR of GBCA of 16 μM was significantly higher than those of the gray or white matter ($p < 0.05$). The optimal TE of the hT2W-FLAIR sequence for detecting very low concentration of GBCA was 700 ms, and the signal intensity of GBCA was higher than that of gray or white matter at the lowest concentration of 16 μM.

✉ Yusuke Sato
ysato@gunma-u.ac.jp

Extended author information available on the last page of the article

1 Introduction

Contrast-enhanced magnetic resonance imaging (MRI) may increase the contrast between lesions and normal tissue, and permit the revealing of several pathologic processes, which would be undetectable without contrast agents or other imaging modalities [1, 2]. The gadolinium (Gd)-based contrast agents (GBCAs) have been used as a positive contrast agent in MRI. Since Gd is a type of heavy metal which is toxic in the form of free ions, chelated Gd has been used as GBCAs to suppress its toxicity. Chelation promotes rapid excretion from the body. Consequently, nephrogenic systemic fibrosis (NSF) has been reported as a serious side effect of GBCA administration in patients with impaired renal function, but the administration of GBCA with macrocyclic chelate to healthy patients has been considered safe [3, 4]. However, several studies have shown Gd deposition in the brain of patients administered GBCA [1, 5–9]. Currently, clinical adverse events in the human body due to Gd deposition in the brain have not been reported. In vitro studies have reported that GBCAs may disrupt the action of thyroid hormone on thyroid receptors of cerebellar Purkinje cells, or in utero exposure to GBCAs may impair memory function and coordination in babies [10, 11]. However, currently, there is no established theory regarding the Gd deposition mechanism, and the safety of GBCA remains controversial.

A quantitative evaluation technique for trace amounts of Gd which can be applied to the human body, is required to elucidate the mechanism of Gd deposition and to evaluate the side effects of GBCAs on the human body. Since several previous studies reported that hyperintensity of the cerebellar dentate nucleus was observed in T1-weighted images, MRI was considered useful for evaluation of Gd deposition. A heavily T2-weight fluid attenuated inversion recovery (IR) (FLAIR) (hT2W-FLAIR) sequence was useful for imaging low concentrations of Gd [12, 13]. FLAIR is a T2-weighted image in which the CSF signal is suppressed by the IR pulse, and has a high sensitivity for detecting lesions in the brain [14]. A heavily T2-weighted image is an MR hydrography that is set to a longer echo time (TE) and displays the only water component with a long T2 value in high contrast with surrounding tissues. This technique is applied to MR cholangiopancreatography, MR urography, MR sialography, MR cisternography, and MR myelography [15–20]. An hT2W-FLAIR is a FLAIR, in which a TE of 500–600 ms is set, and enhances the signal of tissues with long T2 values other than CSF. This imaging technique can show the outflow process of Gd into the CSF after intravenous injection of GBCA [13].

The T1 and T2 values of the brain parenchyma are 615–1002 ms and 69.4–92.1 ms, respectively, and the T1 and T2 values of the CSF are 3836 and 503 ms, respectively [21–23]. The brain parenchyma with short T1 and T2 values shows high signal intensity on T1-weighted images, but low signal intensity on T2-weighted images, especially on heavily T2-weighted images. Since GBCA has a T1-shortening effect and a small T2-shortening effect, CSF with a small amount of GBCA has much longer T2 values than the brain and slightly shorter T1 values than the CSF. Therefore, hT2W-FLAIR has a large transverse magnetization even

at long TE settings, and also the signal is not suppressed by the IR pulse for the CSF. It is necessary to decrease the signal intensity of not only the CSF but also brain parenchyma to visualize a very low concentration of Gd with high signal intensity in an ideal hT2W-FLAIR.

Therefore, we conducted this phantom study to elucidate the lowest concentration of Gd which can be visualized with high contrast by a hT2W-FLAIR. In addition, we aimed to clarify the optimal TE which can visualize very low concentrations of Gd with high signal intensity and decrease the signal intensity of the brain parenchyma and the CSF.

2 Materials and Methods

### 2.1 Phantom Preparation

GBCA-diluted phantoms and phantoms with T1 and T2 values close to those of gray matter (GM), white matter (WM), and CSF were created.

The GBCA phantoms were created by enclosing gadobutrol (Gd-BT-DO3A, Gadovist; Bayer Schering AG, Berlin, Germany) diluted with purified water (purified water, Kenei Pharmaceutical Co., Ltd., Osaka, Japan) in sealable cylindrical plastic containers. Six kinds of phantoms with concentrations of 4, 8, 16, 32, 64, and 128 μM of GBCA were prepared.

A dietary fiber processed food containing water-soluble fiber indigestible dextrin (dietary fiber, Orihiro Co., Ltd., Gunma, Japan) was used to create GM and WM phantoms [24]. A GM phantom was a solution of insoluble dextrin of 10.8 g in purified water of 20.0 g at a concentration of 35 wt%, while a WM phantom was a solution of indigestible dextrin of 16.4 g in purified water of 20.0 g at a concentration of 45 wt%. The T1 values of GM phantom and WM phantom measured by turbo spin echo (TSE)-IR sequence were 696.2 ms and 450.9 ms, respectively, and the T2 values of GM phantom and WM phantom measured by multi-echo TSE sequence were 106.2 ms and 72.8 ms, respectively [25–28].

The CSF phantom was created by encompassing purified water in a plastic container. Each of the created phantoms was fixed in a cylindrical plastic container with a diameter of 10 cm, and the periphery was filled with a polyvinyl alcohol solution (PVA synthetic laundry starch, Daiso Industries Co., Ltd., Hiroshima, Japan). A schematic diagram of the phantom was shown in Fig. 1. The phantoms were left in the examination room for more than half a day so that the temperature reached room temperature (24 °C). Furthermore, the phantoms were left in the magnetic field for 10 min or longer, and the MR images were acquired with the termination of the solution stopped flow.

Fig. 1 Schematic diagram of the phantom that used the search of a null point of the cerebrospinal fluid (CSF) phantom and optimization of echo time. a is the CSF phantom, b is the gray matter phantom, c is the white matter phantom, d is 128 μM gadolinium based contrast agent (GBCA) phantom, e is 64 μM GBCA phantom, f is 32 μM GBCA phantom, g is 16 μM GBCA phantom, h is 8 μM GBCA phantom and, i is 4 μM GBCA phantom. Each of the created phantoms was fixed in a cylindrical plastic container having a diameter of 10 cm, and the periphery was filled with a polyvinyl alcohol solution
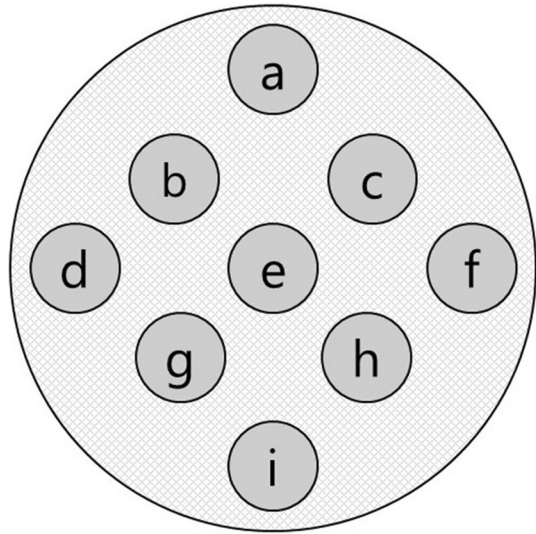
2.2 MRI Acquisition

2.2.1 Optimization of Inversion Time (TI)

IR images of the created phantoms were acquired while changing the TI using a two-dimensional (2D) TSE-IR sequence to determine the null point of the CSF phantom. A 1.5 T MRI scanner (Ingenia 1.5 T, Philips, Amsterdam, Netherlands) with 15-channels head coil was used. TI was changed in 50-ms increments from 1700 to 2100 ms to elucidate the null point of the CSF phantom. The TE was 120 ms, the repetition time (TR) was 8500 ms, the echo train length was 16, the slice thickness was 8 mm, the field of view (FOV) was 128×128 mm, and the matrix size was 256×256. Real images with negative signal intensity were analyzed instead of the magnitude images with absolute values. The region of interest (ROI) was set in the center of the CSF phantom of each IR image as large as possible, and the signal intensity was measured using ImageJ (National Institute of Health, Bethesda, USA, http://imagej.nih.gov/ij). The four data with signal intensities close to zero were used to search the null point of the CSF phantom. From these data points, the optimal TI, at which the signal of the CSF phantom would be zero, was estimated by fitting the relationship between the measured signal intensity and TI to Eq. (1) using the least squares method. The signal intensity of MR images acquired by the IR sequence follows Eq. (1).

$$I(TI) = I_0 \left[1 - 2\exp\left(-\frac{TI}{T_1} \right) \right], \tag{1}$$

where, TI is the inversion time [ms], I(TI) is the signal intensity at TI, I_0 is the initial signal intensity, T1 is the T1 value of the target substance [ms].

2.2.2 Optimization of TE

The FLAIR images of each GBCA phantom were acquired while changing the TE to determine the effect of the TE setting on the signal intensity of these phantoms. A 2D TSE-IR sequence and the same MRI scanner were used to obtain the FLAIR images. The TE was changed by 100-ms increments from 200 to 800 ms. The same sections of the phantom were scanned three times for each TE setting using the dynamic scan mode in which the signal amplification factor remained constant.

2.3 Evaluation

2.3.1 Calculation of CNR

The ROIs were set in the center of each GBCA phantom, brain phantom, and CSF phantom for each scanning setting. The mean and standard deviation of the signal intensity of the ROIs were measured, and the contrast-to-noise ratio (CNR) for the CSF phantom [12] was calculated using Eq. (2).

$$\mathrm{CNR_{CSF}} = \frac{\left|\mathrm{SI} - \mathrm{SI_{CSF}}\right|}{\mathrm{SD_{CSF}}}. \tag{2}$$

Here, SI was the mean signal intensity of the evaluated phantom, $\mathrm{SI_{CSF}}$ was that of the CSF phantom acquired the same TE, and $\mathrm{SD_{CSF}}$ was the standard deviation (SD) of the CSF phantom acquired the same TE.

The three images for each TE were analyzed using the same procedure.

2.3.2 Statistical Analysis

The mean $\mathrm{CNR_{CSF}}$ of each GBCA phantom and GM and WM phantoms were compared for each scan condition. The significance level was set to 5%, and Tukey's multiple comparison method was used. We evaluated the GBCA phantoms that could be visualized when the $\mathrm{CNR_{CSF}}$ of the GBCA phantom was significantly higher than the $\mathrm{CNR_{CSF}}$ of the brain phantom.

3 Results

Figure 2 shows the change of the signal intensity of the CSF phantom in the IR images acquired by changing TI. The null point of the CSF phantom calculated by fitting to Eq. (1) from four data points close to zero was 1920 ms, which was determined to the optimal TI.

Figure 3 shows the FLAIR images acquired while changing TE with TI set to 1920 ms, and Fig. 4 shows the change of the signal intensity at that time. The signal intensity of the GM and WM phantom decreased on extending TE. In contrast, GBCA phantoms ranging from 8 to 128 μM maintained a constant level of signal
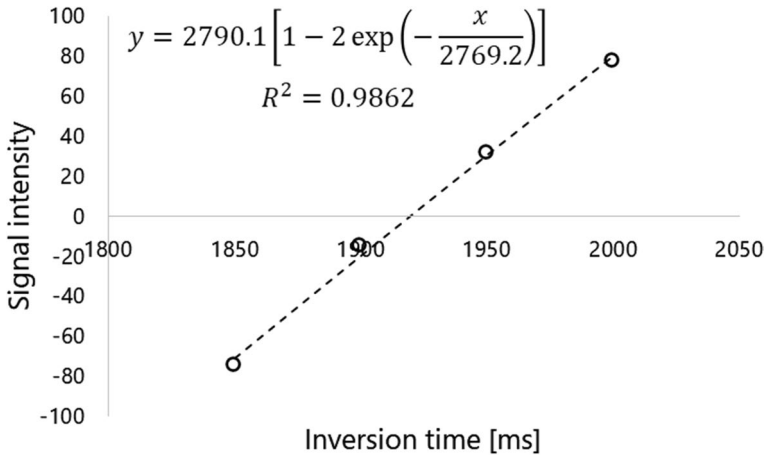
Fig. 2 The changes of signal intensity of the cerebrospinal fluid (CSF) phantom in the inversion recovery images were acquired by changing inversion time. The regression equation fitting to Bloch's equation from four data close to zero was y=2790.1[1−2exp(−x/2769.2)], with a coefficient of determination of 0.9862. The null point of the CSF phantom calculated from the regression equation was 1920 ms
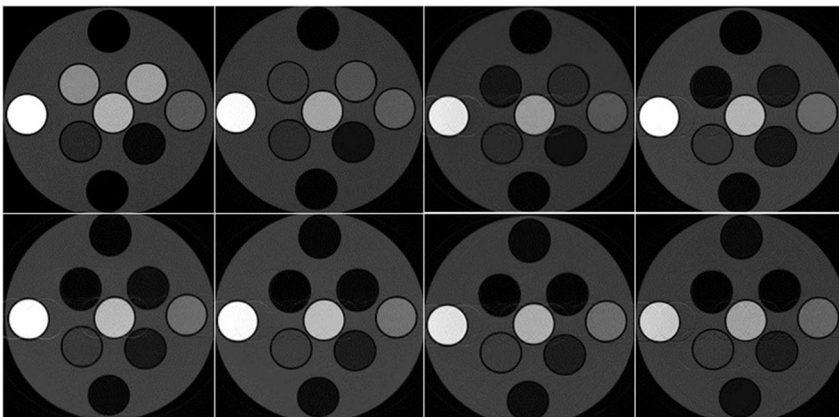
a	b	c	d
e	f	g	h

Fig. 3 The fluid attenuated inversion recovery (FLAIR) images acquired while changing echo time (TE). a is a FLAIR at TE of 100 ms, b is a FLAIR at TE of 200 ms, c is a FLAIR at TE of 300 ms, d is a FLAIR at TE of 400 ms, e is a FLAIR at TE of 500 ms, and f is a FLAIR at TE of 600 ms g is a FLAIR at TE of 700 ms, and h is a FLAIR at TE of 800 ms

intensity even in a long TE setting. The signal intensity of the CSF phantom suppressed by the IR pulse and 4 μM GBCA phantom remained unchanged with a low signal intensity when TE changed.
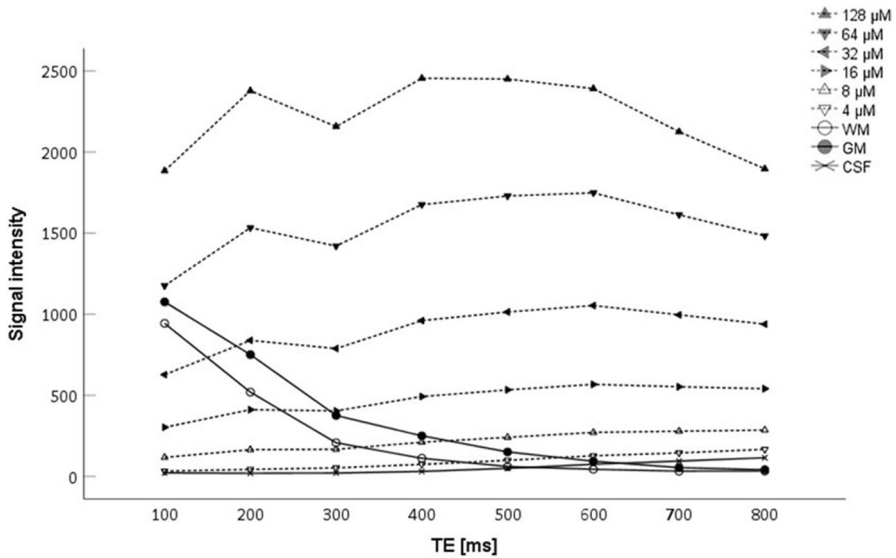
Fig. 4 The changes of signal intensity of each phantom in the fluid attenuated inversion recovery (FLAIR) images acquired by changing echo time (TE). The signal intensity of gray and white matter phantoms decreased steeply by extending TE. On the other hand, the gadolinium-based contrast agent (GBCA) phantoms ranging from 8 to 128 μM maintained a constant level of signal intensity even at a long TE setting. The signal intensity of the CSF phantom suppressed by inversion recovery pulse and 4 μM GBCA phantom remained unchanged with a low signal intensity when TE changed

Table 1 and Fig. 5 shows the change in the CNR_{CSF}, when TE was changed. The CNR_{CSF} of the GM and WM phantoms decreased on extending TE as well as changing the signal intensity. The CNR_{CSF} of the GBCA phantoms peaked at TE of 200 ms. The CNR_{CSF} of GBCA phantoms for 8 to 128 μM were higher than those of the GM and WM phantom at TE of 500 ms. The CNR_{CSF} of relatively high concentrations of GBCA phantoms gradually decreased, but the CNR_{CSF} remained higher than those of GM and WM phantoms at TE of 600–800 ms. The mean of CNR_{CSF} of GBCA phantom and GM phantom were compared for each TE ranging from 500 to 800 ms, since the CNR_{CSF} of GBCA phantoms other than 4 μM were higher than those of the GM and WM phantoms at that TE. As a result, the CNR_{CSF} of the GBCA phantoms was significantly higher than that of the GM at TE of 500–800 ms for 32 to 128 μM ($p < 0.05$). At TE of 700 ms, the CNR_{CSF} of the 16 μM GBCA phantom was significantly higher than that of GM ($p < 0.05$).

4 Discussion

In this study, TE setting did not affect the signal intensity of CSF with the hT2W-FLAIR imaging. Since the hT2W-FLAIR images were acquired using the optimal TI at the null point of CSF signal in advance, it was not surprising that the TE setting did not affect the signal intensity of the CSF phantom.

Table 1 The contrast-to-noise ratio for cerebrospinal fluid (mean ±SD) when the echo time was changed

|	TE [ms]							
	100	200	300	400	500	600	700	800
WM	113.5 ± 6.3	65.6 ± 8.9	18.1 ± 4.6	7.2 ± 1.1	0.8 ± 0.1	2.3 ± 0.8	4.5 ± 0.6	5.5 ± 1.1
GM	129.8 ± 7.2	96.0 ± 12.7	34.4 ± 8.8	19.6 ± 3.8	7.9 ± 0.7	1.3 ± 0.1	2.9 ± 0.6	5.0 ± 1.1
128 μM	229.2 ± 12.5	309.5 ± 40.2	206.5 ± 51.9	216.4 ± 41.5	188.2 ± 22.4*	167.2 ± 35.5*	145.5 ± 15.9*	119.9 ± 17.0*
64 μM	142.0 ± 7.8	198.6 ± 25.8	135.4 ± 34.5	147.0 ± 28.6	131.7 ± 15.8*	120.9 ± 26.1*	108.8 ± 11.8*	92.1 ± 13.3*
32 μM	74.5 ± 4.2	107.5 ± 14.1	74.3 ± 19.2	83.1 ± 16.3	75.6 ± 9.2*	70.7 ± 15.3*	64.6 ± 7.2*	55.5 ± 7.9*
16 μM	34.6 ± 1.8	51.4 ± 6.4	37.0 ± 9.2	41.2 ± 7.7	37.9 ± 4.2	35.5 ± 7.3	32.8 ± 3.4*	28.6 ± 3.9
8 μM	11.8 ± 0.7	19.0 ± 2.2	14.1 ± 3.6	16.1 ± 3.1	15.0 ± 1.6	14.1 ± 2.8	13.2 ± 1.2	11.5 ± 1.4
4 μM	1.4 ± 0.3	3.0 ± 0.2	3.0 ± 0.6	3.8 ± 0.6	3.8 ± 0.1	3.7 ± 0.6	3.6 ± 0.1	3.4 ± 0.3

*$p < 0.05$
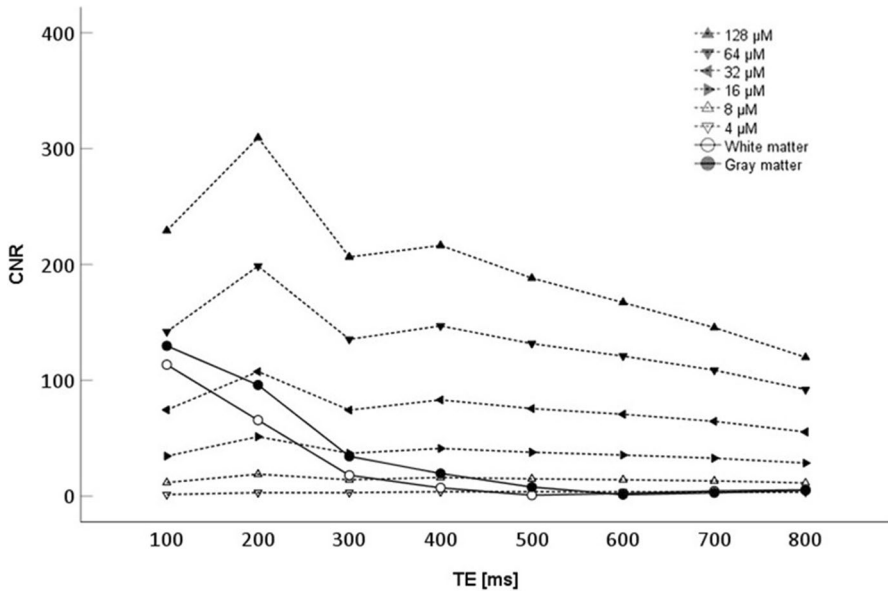
Fig. 5 The change of the contrast-to-noise ratio for cerebrospinal fluid (CNR_{CSF}) when the echo time (TE) was changed. The CNR_{CSF} of gray matter (GM) and white matter (WM) phantoms were decreased by extending TE as well as the change of signal intensity. The CNR_{CSF} of gadolinium-based contrast agent (GBCA) phantoms were peaked at TE of 200 ms. The CNR_{CSF} of GBCA phantoms for 8 to 128 μM were higher than those of GM and WM phantom at TE of 500 ms. The CNR_{CSF} of relatively high concentrations of GBCA phantoms gradually decreased, but the CNR_{CSF} remained higher than those of GM and WM at TE of 600 to 800 ms. The mean of CNR_{CSF} of GBCA phantom and GM phantom were compared for each TE ranging from 500 to 800 ms because the CNR_{CSF} of GBCA phantoms other than 4 μM were higher than those of GM and WM phantoms at that TE. As a result, the CNR_{CSF} of GBCA phantoms were significantly higher than those of the GM at TE of 500 to 800 ms for 32 to 128 μM ($p < 0.05$). Only at TE of 700 ms, the CNR_{CSF} of 16 μM GBCA phantom was significantly higher, compared to those of GM ($p < 0.05$)

The signal intensity of the GM and WM phantom decreased steeply with the extension of the TE. The T1 and T2 values of the GM and WM phantoms were shorter than those of the CSF phantom. The transverse magnetization of a substance with a short T2 value was greatly attenuated in a long TE setting, and the signal intensity was decreased. Therefore, the signal intensity of the GM and WM phantoms also decreased with the extension of TE.

In contrast, the signal intensity of the GBCA phantoms did not decrease greatly and remained constant even at long-TE settings. The GBCA phantoms consisted of purified water with long T1 and T2 values and a very small amount of GBCA with a T1 and T2 shortening effect. Therefore, the GBCA phantoms have slightly shorter T1 and T2 values than the CSF phantom. The signal intensity of the GBCA phantoms was not suppressed by the IR pulse, since the T1 values of these phantoms were slightly different from that of the CSF phantom. In addition, the attenuation of the transverse magnetization of the GBCA phantoms with a long T2 value was smaller than those of the GM and WM phantoms, even at long TE settings.

Therefore, the signal intensity of the GBCA phantoms did not decrease as in the GM and WM phantoms, upon the exceeding TE (Fig. 6).

The signal intensity of GM and WM phantoms was lower than that of 64 μM and 128 μM GBCA phantoms at a TE of 100 ms, 32 μM GBCA phantom at 200 ms, 16 μM GBCA phantom at 300–400 ms, and 8 μM GBCA phantom at 500–800 ms. Thus, the signal intensity of even lower concentrations of Gd became higher than that of the brain parenchyma when TE was extended. An hT2W-FLAIR sequence makes it possible to image low concentrations of Gd with high contrast by utilizing this signal value reversal between Gd and the brain parenchyma. In addition, Gd must be present in the tissue with a very long T2 value to visualize Gd with high contrast by using hT2W-FLAIR. It has been reported that a hT2W-FLAIR can visualize the perivascular space with high contrast and the outflow process of Gd into the CSF after intravenous injection of GBCA [13]. The reason the hT2W-FLAIR made this possible was that Gd was present in the CSF and the interstitial fluid with a long T2 value. Therefore, the hT2W-FLAIR may also trace Gd in the perivascular space and be useful for elucidating the glymphatic system. In contrast, the observation of Gd deposition in the brain parenchyma with a short T2 value was expected to be difficult.

In this study, the lowest imaging limit of the GBCA concentration was 16 μM. TI value was tried to make the CSF signal null, but 4 μM and 8-μM GBCA signals
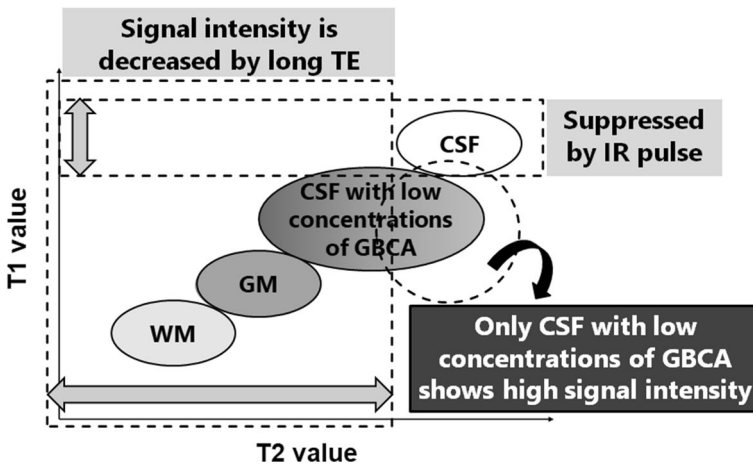

Fig. 6 An imaging principle of the heavily T2-weighted fluid attenuated inversion recovery (FLAIR) (hT2W-FLAIR) sequence. In hT2W-FLAIR, the cerebrospinal fluid (CSF) was suppressed by inversion recovery (IR) pulse, and the signal intensity of the gray matter (GM) and white matter (WM) was decreased by long echo time (TE) setting. On the other hand, the signal intensity of gadolinium-based contrast agent (GBCA) phantoms did not decrease greatly and maintained a constant level even at long TE settings. The GBCA phantoms have slightly shorter T1 and T2 values than the CSF phantom. The signal intensity of GBCA phantoms are not suppressed by IR pulse because the T1 values of these phantoms are slightly different from the CSF phantom. Also, the attenuation of transverse magnetization of GBCA phantoms with long T2 value are smaller than those of GM and WM phantoms even at long TE settings. Therefore, the signal intensity of the GBCA phantoms did not decrease like the GM and WM phantoms by exceeding TE. Therefore, the GBCA presenting in the tissue having long T2 value such as CSF was visualized with high contrast

were also suppressed by IR pulses. The signal of the tissues with T1 values close to CSF may also be suppressed by the IR pulse. It is possible to depict low-concentration GBCA by setting the IR pulse more accurately so that the signal of the low-concentration GBCA with a slightly different T1 relaxation time is not suppressed.

Naganawa et al. reported that the optimal TE was 500–600 ms in GBCA phantoms diluted 4000–32,000 times dimeglumine (Gd-DTPA, Magnevist; Bayer, Osaka, Japan) (concentrations were 15.6–125 μM) by using a 3D sequence at 3.0 T MRI scanner [12]. In this study, it was possible to visualize a similar 16 μM GBCA despite using a more general 2D sequence of a 1.5 T MRI. In addition, our study suggested that it was possible to decrease the signal intensity of the brain parenchyma while maintaining Gd sensitivity by extending TE at 700 ms in 1.5 T MRI. The decrease of the brain parenchymal signal may improve the contrast between Gd and the brain parenchyma, and allow the visualization of lower concentrations of Gd. The 3D sequences used in previous studies are generally complicated in structure and settings and largely depend on the base sequence and the MRI manufacturer. We clarified the basic characteristics of the hT2W-FLAIR and demonstrated that the hT2W-FLAIR can be acquired even with a 2D sequence of a 1.5 T MRI. This result will greatly contribute to the spread and development of a hT2W-FLAIR. Furthermore, we suspected that it may lead to the elucidation of the glymphatic system and the mechanism of brain Gd deposition, providing safer contrast-enhanced MRI examinations.

Our study had several limitations. The purified water used for the CSF phantom had a composition different from the CSF, which contained multiple ions, proteins, etc. [29]. Therefore, purified water may have a lower T1 value than that of *in-vivo* CSF [30]. TI was the optimum value for suppressing the signal of purified water; it may not be the TI for the actual CSF. If this sequence is applied clinically, it is necessary to follow the same procedure as this study, and a new accurate TI for the CSF is to be set. The created phantoms can reproduce almost the human body, but the T1 and T2 values of the actual human brain include individual differences [21, 31–33]. Since there was only one set of phantoms in this study, the effects of the variations in T1 and T2 values of the brain could not be evaluated. TE and TI that contribute to image contrast were examined, but other scanning parameters such as resolution or slice thickness were also required for clinical application.

5 Conclusion

The optimal TE of the hT2W-FLAIR sequence for detecting a very low concentration of GBCA was 700 ms, and the lowest detectable concentration of GBCA was 16 μM.

Declarations

Competing interests The authors declare no competing interests.

Conflict of Interest The authors declare that they have no conflicts of interest.

References

1. R.J. McDonald, J.S. McDonald, D.F. Kallmes, M.E. Jentoft, D.L. Murray, K.R. Thielen et al., Intracranial gadolinium deposition after contrast-enhanced MR imaging. Radiology **275**(3), 772–782 (2015)
2. A.A.P. Kartamihardja, H. Hanaoka, P. Andriana, S. Kameo, A. Takahashi, H. Koyama et al., Quantitative analysis of Gd in the protein content of the brain following single injection of gadolinium-based contrast agents (GBCAs) by size exclusion chromatography. Br. J. Radiol. **92**(1099), 20190062 (2019)
3. T. Grobner, Gadolinium—a specific trigger for the development of nephrogenic fibrosing dermopathy and nephrogenic systemic fibrosis? Nephrol. Dial. Transplant. **21**(4), 1104–1108 (2006)
4. W.A. High, R.A. Ayers, J. Chandler, G. Zito, S.E. Cowper, Gadolinium is detectable within the tissue of patients with nephrogenic systemic fibrosis. J. Am. Acad. Dermatol. **56**(1), 21–26 (2007)
5. T. Kanda, K. Ishii, H. Kawaguchi, K. Kitajima, D. Takenaka, High signal intensity in the dentate nucleus and globus pallidus on unenhanced T1-weighted MR images: relationship with increasing cumulative dose of a gadolinium-based contrast material. Radiology **270**(3), 834–841 (2014)
6. Y. Zhang, Y. Cao, G.L. Shih, E.M. Hecht, M.R. Prince, Extent of signal hyperintensity on unenhanced T1-weighted brain MR Images after more than 35 administrations of linear gadolinium-based contrast agents. Radiology **282**(2), 516–525 (2017)
7. Y. Errante, V. Cirimele, C.A. Mallio, V. Di Lazzaro, B.B. Zobel, C.C. Quattrocchi, Progressive increase of T1 signal intensity of the dentate nucleus on unenhanced magnetic resonance images is associated with cumulative doses of intravenously administered gadodiamide in patients with normal renal function, suggesting dechelation. Invest. Radiol. **49**(10), 685–690 (2014)
8. A. Radbruch, L.D. Weberling, P.J. Kieslich, O. Eidel, S. Burth, P. Kickingereder et al., Gadolinium retention in the dentate nucleus and globus pallidus is dependent on the class of contrast agent. Radiology **275**(3), 783–791 (2015)
9. T. Kanda, M. Osawa, H. Oba, K. Toyoda, J. Kotoku, T. Haruyama et al., High signal intensity in dentate nucleus on unenhanced T1-weighted MR images: association with linear versus macrocyclic gadolinium chelate administration. Radiology **275**(3), 803–809 (2015)
10. W. Ariyani, T. Iwasaki, W. Miyazaki, E. Khongorzul, T. Nakajima, S. Kameo et al., Effects of gadolinium-based contrast agents on thyroid hormone receptor action and thyroid hormone-induced cerebellar Purkinje cell morphogenesis. Front. Endocrinol. (2016). https://doi.org/10.3389/fendo.2016.00115
11. M.A. Khairinisa, Y. Takatsuru, I. Amano, K. Erdene, T. Nakajima, S. Kameo et al., The effect of perinatal gadolinium-based contrast agents on adult mice behavior. Invest. Radiol. **53**(2), 110–118 (2018)
12. S. Naganawa, H. Kawai, M. Sone, T. Nakashima, Increased sensitivity to low concentration gadolinium contrast by optimized heavily T2-weighted 3D-FLAIR to visualize endolymphatic space. Magn. Reason. Med. Sci. **9**(2), 73–80 (2010)
13. S. Naganawa, T. Nakane, H. Kawai, T. Taoka, Gd-based contrast enhancement of the perivascular spaces in the basal Ganglia. Magn. Reason. Med. Sci. **16**(1), 61–65 (2017)
14. A.H. Herlihy, J.V. Hajnal, W.L. Curati, N. Virji, A. Oatridge, B.K. Puri et al., Reduction of CSF and blood flow artifacts on FLAIR images of the brain with k-space reordered by inversion time at each slice position (KRISP). AJNR Am. J. Neuroradiol. **22**(5), 896–904 (2001)

15. J.C. Varghese, R.P. Liddell, M.A. Farrell, F.E. Murray, D.H. Osborne, M.J. Lee, Diagnostic accuracy of magnetic resonance cholangiopancreatography and ultrasound compared with direct cholangiography in the detection of choledocholithiasis. Clin. Radiol. **55**(1), 25–35 (2000)

16. J.A. Waters, C.M. Schmidt, J.W. Pinchot, P.B. White, O.W. Cummings, H.A. Pitt et al., CT vs MRCP: optimal classification of IPMN type and extent. J. Gastrointest. Surg. **12**(1), 101–109 (2008)

17. J. Abreu-Gomez, A. Udare, K.P. Shanbhogue, N. Schieda, Update on MR urography (MRU): technique and clinical applications. Abdominal Radiol. **44**(12), 3800–3810 (2019)

18. Y. Takagi, M. Sumi, T. Sumi, Y. Ichikawa, T. Nakamura, MR microscopy of the parotid glands in patients with Sjögren's syndrome: quantitative MR diagnostic criteria. Am. J. Neuroradiol. **26**(5), 1207–1214 (2005)

19. T. El Gammal, W. Sobol, V.R. Wadlington, M.J. Sillers, C. Crews, W.S. Fisher et al., Cerebrospinal fluid fistula: detection with MR cisternography. Am. J. Neuroradiol. **19**(4), 627–631 (1998)

20. H.-M. Yoo, S.J. Kim, C.G. Choi, D.H. Lee, J.H. Lee, D.C. Suh et al., Detection of CSF leak in spinal CSF leak syndrome using MR myelography: correlation with radioisotope cisternography. Am. J. Neuroradiol. **29**(4), 649–654 (2008)

21. S.C.L. Deoni, B.K. Rutt, T.M. Peters, Rapid combined T1 and T2 mapping using gradient recalled acquisition in the steady state. Magn. Reson. Med. **49**(3), 515–526 (2003)

22. H. Lu, L.M. Nagae-Poetscher, X. Golay, D. Lin, M. Pomper, P.C.M. van Zijl, Routine clinical brain MRI sequences for use at 3.0 Tesla. J. Magn. Reason. Imaging **22**(1), 13–22 (2005)

23. S.K. Piechnik, J. Evans, L.H. Bary, R.G. Wise, P. Jezzard, Functional changes in CSF volume estimated using measurement of water T2 relaxation. Magn. Reson. Med. **61**(3), 579–586 (2009)

24. A. Yamashiro, M. Kobayashi, T. Saito, Cerebrospinal fluid T1 value phantom reproduction at scan room temperature. J. Appl. Clin. Med. Phys. **20**, 166–175 (2019)

25. R. Rakow-Penner, B. Daniel, H. Yu, A. Sawyer-Glover, G.H. Glover, Relaxation times of breast tissue at 1.5T and 3T measured using IDEAL. J. Magn. Reason. Imaging **23**(1), 87–91 (2006)

26. F.E. Mozes, E.M. Tunnicliffe, M. Pavlides, M.D. Robson, Influence of fat on liver T1 measurements using modified Look-Locker inversion recovery (MOLLI) methods at 3T. J. Magn. Reson. Imaging **44**(1), 105–111 (2016)

27. D. Kim, J.H. Jensen, E.X. Wu, S.S. Sheth, G.M. Brittenham, Breathhold multiecho fast spin-echo pulse sequence for accurate R2 measurement in the heart and liver. Magn. Reson. Med. **62**(2), 300–306 (2009)

28. N. Ben-Eliezer, D.K. Sodickson, K.T. Block, Rapid and accurate T2 mapping from multi–spin-echo data using Bloch-simulation-based reconstruction. Magn. Reson. Med. **73**(2), 809–817 (2015)

29. P.D. Brown, S.L. Davies, T. Speake, I.D. Millar, Molecular mechanisms of cerebrospinal fluid production. Neuroscience **129**(4), 955–968 (2004)

30. A. Yamashiro, M. Kobayashi, T. Saito, Cerebrospinal fluid T1 value phantom reproduction at scan room temperature. J. Appl. Clin. Med. Phys. **20**(7), 166–175 (2019)

31. K.P. Whittall, A.L. Mackay, D.A. Graeb, R.A. Nugent, D.K.B. Li, D.W. Paty, In vivo measurement of T2 distributions and water contents in normal human brain. Magn. Reson. Med. **37**(1), 34–43 (1997)

32. J.P. Wansapura, S.K. Holland, R.S. Dunn, W.S. Ball Jr., NMR relaxation times in the human brain at 3.0 tesla. J. Magn. Reson. Imaging **9**(4), 531–538 (1999)

33. G.J. Stanisz, E.E. Odrobina, J. Pun, M. Escaravage, S.J. Graham, M.J. Bronskill et al., T1, T2 relaxation and magnetization transfer in tissue at 3T. Magn. Reson. Med. **54**(3), 507–512 (2005)

Authors and Affiliations

Yusuke Sato[1,2] · Norio Hayashi[3] · Kouichi Ujita[1] · Takayuki Suto[1] · Haruyuki Watanabe[3] · Yoshito Tsushima[4]

[1] Department of Radiology, Gunma University Hospital, 3-39-15 Showa, Maebashi, Gunma 371-8511, Japan

[2] Department of Radiological Technology, Graduate School of Radiological Technology, Gunma Prefectural College of Health Sciences, 323-1 Kamioki, Maebashi, Gunma 371-0052, Japan

[3] Department of Radiological Technology, Gunma Prefectural College of Health Sciences, 323-1 Kamioki, Maebashi, Gunma 371-0052, Japan

[4] Department of Diagnostic Radiology and Nuclear Medicine, Gunma University Graduate School of Medicine, 3-39-15 Showa, Maebashi, Gunma 371-8511, Japan